

Interaction of DNA with CNTs: Properties and Prospects for Electronic Sequencing

SHENG MENG and EFTHIMIOS KAXIRAS

Department of Physics and School of Engineering and Applied Sciences,
Harvard University, Cambridge, Massachusetts

- 3.1 Introduction
- 3.2 Structural properties of combined DNA–CNT systems
 - 3.2.1 single nucleotide on a CNT
 - 3.2.2 DNA oligomers on a CNT
 - 3.2.3 Helix of DNA on a CNT
 - 3.2.4 Integration of DNA and a CNT array
 - 3.2.5 DNA inside CNT pores
- 3.3 Electronic structure
 - 3.3.1 Polarization and charge transfer
 - 3.3.2 Density of states
 - 3.3.3 STM images
- 3.4 Optical properties
- 3.5 Biosensing and sequencing of DNA using CNTs
 - 3.5.1 Gaseous sensing using DNA–CNT
 - 3.5.2 Field-effect transistor and optical shift for DNA detection
 - 3.5.3 Monitoring morphology changes of dsDNA
 - 3.5.4 DNA sequencing
- 3.6 Summary

3.1 INTRODUCTION

The interaction between DNA and carbon nanotubes (CNTs) is a subject of intense current interest. Both DNA strands and CNTs are prototypical one-dimensional structures; the first plays a central role in biology, and the second holds promise for an equally pivotal role in nanotechnology applications. Single-stranded DNA (ssDNA) and CNTs have complementary structural features that make it possible to assemble them into a stable hybrid structure: ssDNA is a flexible, amphiphilic biopolymer, whereas CNTs are stiff, strongly hydrophobic nanorods. Indeed, ssDNA of different lengths, either small oligomers consisting of tens of bases [1,2] or long genomic strands (ca.100 bases) [3], wrap-around single-walled CNTs, forming tight helices, as observed by atomic force microscopy (AFM). Similarly, double-stranded DNA (dsDNA) [4,5] and fragmented dsDNA (a hybrid of both ssDNA and dsDNA) [6] can also be associated with a CNT, although less efficiently. In addition, as predicted theoretically [7,8] and confirmed experimentally [9] by high-resolution transmission electron microscopy (TEM), DNA can be encapsulated into the CNT interior.

Although the structures of DNA and CNTs, each in its natural form and environment, are well established (e.g., the B-DNA form in solution [10] or isolated CNTs [11]), the molecular structure for the combined DNA–CNT systems is not well characterized, and the nature of their interaction remains elusive [1–4,12–17]. This has motivated many studies and possible applications. For instance, it has been inferred from optical spectra that double-stranded DNA experiences a conformational transformation from the B-form to the Z-form on the CNT surface with the increase in ion concentration [4]. Due to their intriguing properties, including 100-fold-higher tensile strength than steel, excellent thermal conductivity comparable to that of diamond, and tunable electric conductance, CNTs have been proposed as the template for DNA encapsulation [9], intracellular DNA transport [13], DNA hybridization [17], and electrochemical DNA detection [12]. A different set of applications involves ssDNA wrapping around CNTs in a diameter- and sequence-dependent manner, which would make it possible to dissolve the naturally hydrophobic single [18] or multiwalled CNTs in water [19] and to sort them by their chirality [1,2]. Finally, DNA-decorated CNTs have been examined as a chemical sensor to discriminate odors in air [14] and glucose in solution [5], while DNA strands in contact with a CNT array have been proposed as the basis for electronic switches involving electron transport in both components [15] and for high-*k*-dielectric field-effect transistors (FETs) [20].

There is also an increasing interest in the use of CNTs for supporting and detecting DNA through electronic [16] and optical means [4,17], which could lead to ground-breaking, ultrafast DNA sequencing at low cost (see Figure 3.1 for a hypothetical setup), approaching the target of \$1000 per genome. Previous studies show that electronic detection of DNA bases using transverse conductance measurements depends sensitively on the tip-base distance and relative orientation, factors that can overwhelm the signal dependence on base identity and severely limit the efficacy of single-base detection methods [21–23]. These difficulties may

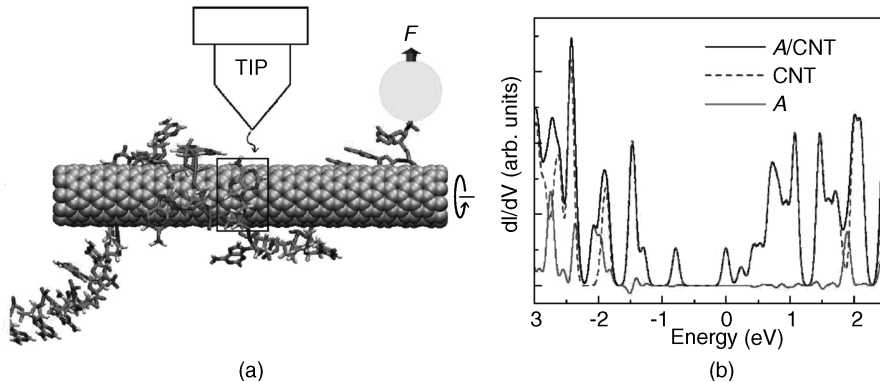


FIGURE 3.1 (a) Theoretical proposal for a setup for electronic DNA sequencing using partially DNA-wrapped CNTs and a probe with atomic-scale resolution, such as scanning tunneling spectroscopy. (b) The differential current–voltage curves are shown for the combined system (black line) and bare CNT (dashed); their difference (gray) corresponds to the measured signal for the DNA base under the tip (the example corresponds to the base A).

be overcome in the combined DNA–CNT system, since as we discuss later, attaching DNA on a CNT fixes the geometry of nucleotide (both the base–CNT distance and base orientation) on the CNT wall. Indeed, recent success in detecting DNA conformational changes [4] and hybridization [17] by near-infrared fluorescence of CNTs or CNT-field-effect transistors [16] opened the door for DNA sequencing based on its electronic structure.

To this end, what is currently missing for practical DNA detection and sequencing on CNTs is a detailed understanding of the nature of the DNA–CNT interaction and its dependence on the nucleotide identity. The DNA–CNT hybrid is a complicated, dynamic structure in which the four types of bases [the two purines, adenine (A) and guanine (G), and the two pyrimidines, cytosine (C) and thymine (T)] interact with the CNT in the presence of thermal fluctuations. Individual DNA bases can be stabilized on CNTs through mainly weak van der Waals interaction to the graphitic CNT wall. This interaction is perturbed by the sugar and phosphate groups in the DNA backbone, the counterions that bind to DNA, and the water molecules from solution. Even if the idea of using CNT as a template to hold and fix the DNA bases for electronic detection appears promising, many issues remain to be resolved before it is proven practical. The fundamental aspects of the DNA–CNT interaction include binding geometries, base orientation, mutual polarization, charge transfer, DNA association and dissociation, dynamical structure evolution, and response to electric and optical signals; all these need to be addressed at the molecular level. The dependence of these properties on the base identity, once explicitly resolved, may lead to the development of new DNA sequencing methods. We review here the properties of DNA–CNT systems and discuss the prospects for DNA detection and sequencing using electronic signals from CNTs.

3.2 STRUCTURAL PROPERTIES OF COMBINED DNA–CNT SYSTEMS

3.2.1 Single Nucleotide on a CNT

The first step in attempting to understand the DNA–CNT interaction is to establish the possible binding geometries in a DNA–CNT system, beginning with the structure of a single nucleotide adsorbed on the CNT surface [24]. To study this local interaction, we have used nucleosides, consisting of a base, a deoxyribose sugar group, and terminated by OH at the 3' and 5' ends. The phosphate group of a nucleotide is not included (in the following we identify nucleotides by the same symbols as the bases). We use the semiconducting (10,0) nanotube, which is abundant during synthesis and has a diameter of 7.9 Å, as a representative example of CNTs. We determined the energetically favorable configurations of the bases on the nanotube with the CHARMM program [25] using standard force fields [26] for atoms comprising the nucleosides and force fields of aromatic carbon atoms for those belonging to the CNT.

Compared to the planar structure of graphite, CNTs have a curved structure that perturbs only slightly the nucleoside adsorption positions but results in many inequivalent adsorption geometries. We performed an extensive search of the potential energy surface of each adsorbed nucleoside using the successive confinement method [27]. The potential energy surfaces of biomolecules are extremely complicated [28] and currently preclude direct exploration with *ab initio* methods. The search returned approximately 1000 distinct potential energy minima for each base–CNT system, with the global energy minimum structures shown in Figure 3.2(a). The room-temperature populations of each minimum range from 10^{-10} to 50%. Despite the numerous configurations, we found that very few of them are dominant, with significant room-temperature populations. For instance, there are four most stable configurations for C, with populations 25.2, 6.8, 4.3, and 3.2% [shown in Figure 3.2(b)]. Similarly, there are three dominant configurations for A, with populations of 28.4, 27.6,

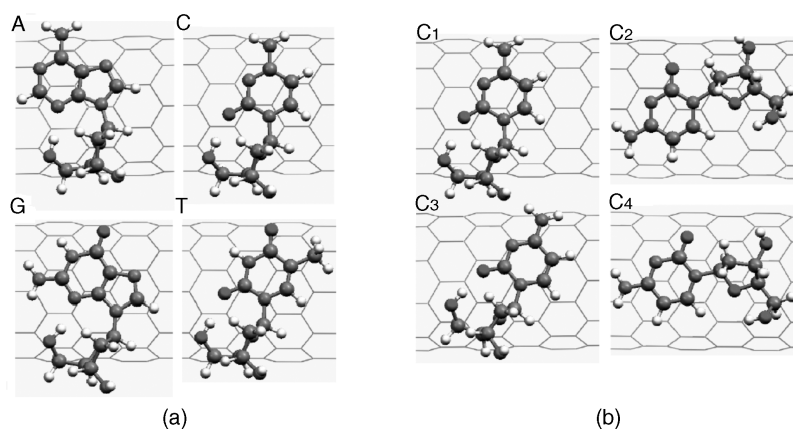


FIGURE 3.2 (a) The most stable configuration for a single nucleoside adsorption on the (10,0) CNT; (b) the four most stable configurations for adsorption of C on the CNT.

and 10.1%; three configurations for G (populations: 45.9, 20.8, and 7.2%), and four for T (populations: 11.2, 5.0, 4.1, and 2.0%). Together, these three to four structures represent the majority of the total population of configurations. The rest of the population contains more than 800 configurations. Therefore, it is reasonable to focus only on the dominant configurations in our evaluation of the DNA–CNT interactions. This is particularly true when we show later that the various configurations make a negligible difference in the DNA–CNT interaction.

The preferred configurations for each base have certain similarities, but all are different from their ideal geometries upon adsorption on a planar graphene layer. The nucleoside binds on carbon nanotubes through its base unit, located 3.3 Å away from the CNT wall. Whereas the base unit remains planar without significant bending, the sugar residue is more flexible. It lies farther away from the CNT, usually having its OC₄ plane perpendicular to the CNT wall with the O atom pointing toward it (Figure 3.2). On a graphene layer, the N and C atoms of A are found to occupy the hollow sites of the hexagonal rings, resembling AB stacking between adjacent layers in graphite [29]. Here, however, because of the curvature of the CNT, the C and N atoms of the base do not necessarily reside on the top of hexagonal C rings; instead, they can shift positions to maximize the attraction between C, N, and O atoms in the base and C atoms in the CNT. For guanine and cytosine on graphene, there is already a significant deviation from AB stacking [30]; they are further displaced on the CNT wall, with G being closest to that on the graphene structure, shifted by only about 0.8 Å along one C–C bond and slightly rotated. Moreover, because the CNT structure is highly asymmetric with a long axis, the orientation of a base with respect to the tube axis can be very different. For instance, in the four preferred geometries for C, two are rotated by about 90° relative to the most stable configuration (Figure 3.2). Interestingly, all four of the most stable configurations involving nucleoside adsorption on the CNT have the sugar-base direction pointing perpendicular to the tube axis or slightly tilted.

The force-field approach discussed so far relies on empirically derived dispersion interactions. In the context of the quantum approach, it is the explicit polarization of electronic charge that contributes to interaction between the nucleosides and the CNT. The structures obtained from the force-field calculations were further optimized using density functional theory in the local density approximation (LDA) for the exchange-correlation functional [31]. The structural relaxation was carried to the point where the forces calculated on each atom have a magnitude smaller than 0.005 eV/Å. The local structure, that is, covalent bond lengths and bond angles, shows little deviation from that obtained with the force field (of order 0.02 Å and 1°), while the optimal CNT–base distance is reduced by about 0.3 Å. The base adsorption induces a very small distortion of the CNT geometry, consisting of a 0.02-Å depression on the adsorption side and a 0.007-Å protrusion on the opposite side. The interaction energy calculated is 0.43 to 0.46 eV for the four nucleosides. This value is very close to the LDA calculation of adenine on graphite (0.46 eV) [29], but is significantly lower than the van der Waals energy of 0.70 to 0.85 eV from the CHARMM calculations (0.70 eV for C, 0.77 eV for T, 0.81 eV for A, and 0.85 eV for G). In comparison, the experimental value extracted from thermal desorption spectroscopy for adenine on graphite is

1.01 eV [32], which is reasonably close to the sum of the dispersion and electronic interaction energies (1.13 eV).

3.2.2 DNA Oligomers on a CNT

After examining the interaction between a single nucleoside and CNT, the next natural step is the interaction of a nucleotide strand with CNT, where the competition between the base–base and the base–CNT interactions comes into play. Using classic molecular dynamics (MD) simulations based on CHARMM force fields, we have investigated the interaction between CNTs and DNA oligomers, that is, short DNA strands consisting of a few bases and up to tens of DNA bases. The simulation box, of dimensions $25 \text{ \AA} \times 25 \text{ \AA} \times 43.4 \text{ \AA}$, comprises a DNA oligomer, a CNT (10,0), and about 700 water molecules with sodium counterions to neutralize the DNA backbone. We employ the TIP3P water model and periodic boundary conditions [33]. Constant pressure and constant temperature are controlled by the Berendsen barostat and the Nose–Hoover thermostat [34], respectively, toward the target values of 1 bar and 300 to 400 K. The particle-mesh Ewald method with cubic spline interpolation [35] is used to evaluate electrostatic energies and forces. A time step of 2 fs is used, and the OH vibrations are frozen using the SHAKE algorithm. The full trajectory is recorded every 1 ps after an equilibration of 20 to 200 ps.

Figure 3.3 shows the association dynamics of a ssDNA oligomer consisting of six adenine bases [poly(dA₆)] with the CNT, at 300 K during a period of 3 ns. Initially, each base is 5 to 9 Å away from the nanotube outer surface. Here the base–CNT distance is defined as the distance between the center of mass of the individual base and the CNT wall. After 5 ps, one base at one of the two ends of the strand (base 1) quickly starts to attach on the CNT surface, as evidenced by a base–CNT distance of 3.4 Å. The other bases gradually approach the CNT wall. At time $t = 0.545 \text{ ns}$ and $t = 0.575 \text{ ns}$, respectively, the fourth and fifth bases counted from the same end of ssDNA attach to the CNT surface and are stabilized there. The rest of the DNA bases either stack on top of these CNT-attached bases (e.g., base 6) or are stacked among themselves (bases 2 and 3), forming a bubble on the CNT, as shown in the snapshot at 0.6 ns. Similar events take place at $t = 0.7$ to 0.8 ns for bases 2 and 3, when the base stacking is broken and both bases adsorb on the CNT surface. At this time, the system reaches steady state, where five of six bases form a close contact with the CNT surface, lying flat at a distance of 3.4 Å, which helps optimize the van der Waals attraction between the base and the CNT. Occasionally, some bases flip up, resulting in the base plane being aligned vertically with the CNT wall, which is followed by a larger oscillation in the base–CNT distance above 4 Å. The last base, base 6, at the other end of the ssDNA strand, forms a very stable stacking on base 5 during the $t = 0.8$ to 1.9 ns time interval [Figure 3.3(d)]. This stacking is not broken until 1.9 ns. After that, the DNA oligomer forms a stable horseshoe-like structure with all bases stacked on the CNT wall without self-stacking, which lasts for at least another nanosecond. The large deviation in the base–CNT distance for base 4 is due to its frequent flipping up and back onto the CNT wall. During the ssDNA–CNT association

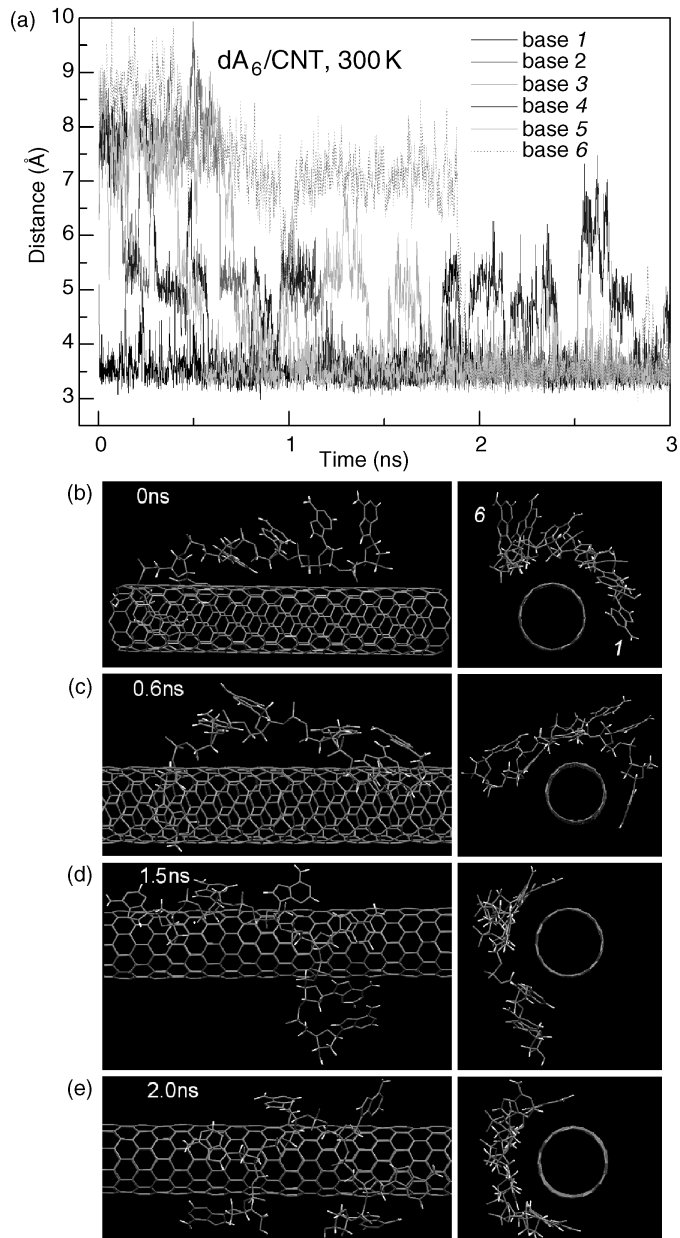


FIGURE 3.3 (a) Distance between the center of mass of each base in the ssDNA oligomer dA_6 and the CNT wall as a function of the simulation time; (b–e) snapshots from the simulation trajectory at times of 0, 0.6, 1.5, and 2.0 ns, respectively. Two views from directions vertical and parallel to the CNT axis are shown. For clarity, water molecules and counterions are not shown.

process, there is a stepwise decrease in the base–CNT distance; the terraces correspond to metastable intermediate states in which some bases are stacked between themselves.

The association of ssDNA on CNT walls in aqueous solution is due to both the hydrophobic effect and the vdW interaction, with the latter playing a dominant role. The interaction energy between the DNA base plane and the CNT wall is much larger than the self-stacking energy of bases: In Figure 3.4(a) we compare base–base interaction and a base–CNT stacking energy during the simulation, for the case of adenine. The A–CNT interaction energy is around 0.50 eV, larger than the A–A stacking energy by roughly a factor of 2. The presence of the sugar and phosphate group adds about another 0.3 eV to the total van der Waals interaction energy between the nucleotide and the CNT (not shown in this figure). The hydrophobic effect comes from the fact that the bases in DNA strands are hydrophobic and are likely to form a hybrid with the highly hydrophobic CNTs.

The process above is observed for other ssDNA strands of different sequence and length and should be considered as a general characteristic for ssDNA–CNT association. There exist, however, many stable ssDNA–CNT structures, among which the horseshoe structure is one of the most stable, observed for other oligomers, including poly(dG6) and poly(dC6). Other stable structures include the DNA strand linearly aligned along the nanotube axis, the S-shaped structure on the CNT wall, or a part of a helix structure. In our simulations, a six-base strand is too short to form a full period of a helix on the CNT. We also find that the base–CNT stacking and base–base stacking coexist in the stable ssDNA–CNT structures. The stacking of bases among themselves can occur either at the end of the ssDNA strand or in the middle, forming “bubbles” 5 to 8 Å high on the CNT. There is a relatively large barrier for these structures to develop optimal contact with the CNT (all bases lying flat and close to the CNT wall); therefore, they can be considered as “metastable” states, and do not unfold fully in our short simulations at the nanosecond scale.

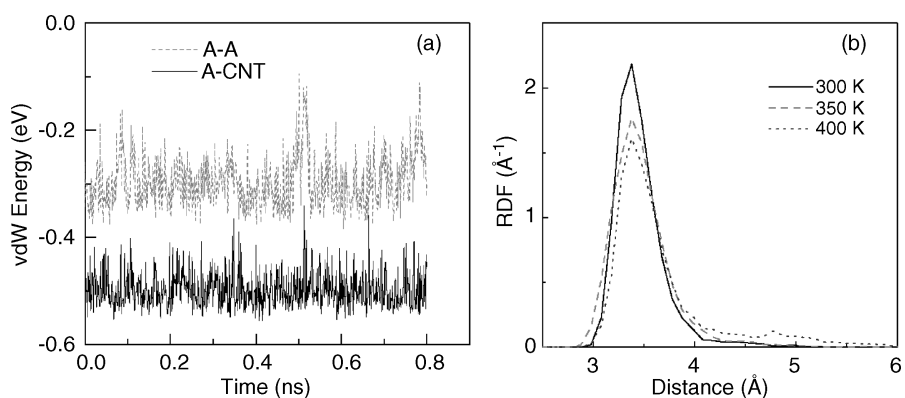


FIGURE 3.4 (a) Van der Waals interaction energy between base and CNT and between base and base in the simulation of dA_6/CNT in water; (b) radial distribution function of dA_6/CNT at different temperatures.

At different temperatures, the bound DNA–CNT structure exhibits different stability. When increasing the temperature, some bases are more likely to deviate from the optimal adsorption position and to detach from the CNT wall. Figure 3.4(b) shows the radial distribution function of the center of mass of each base around the CNT wall at different temperatures, averaged over all six bases in a 1-ns trajectory starting from the same configuration, which is the optimal contact between each DNA base and CNT. These results indicate that the higher the temperature, the less tight the ssDNA structure around the CNT, as is evident from the increasing values in the tail of the distribution (larger distances). The probability for a base to stay at the CNT surface actually decreases from 97% at 300 K to 81% at 400 K.

3.2.3 Helix of DNA on a CNT

The longer ssDNA strand will bind on the CNT surface in the same manner as DNA oligomers. Due to its extent, some new structural characteristics arise. The most striking feature is perhaps the formation of a stable, tight helical structure of ssDNA on the CNT along the tube axis, as seen in experiment: Zheng et al. [1] first observed that a relatively short ssDNA strand with 30 to 90 bases can effectively disperse the indissoluble CNT bundles in water after ultrasound sonication. In high-resolution AFM images, the dispersed CNT samples show clearly the helical ssDNA structure upon a single CNT with a constant periodicity along its axis (Figure 3.5). The dispersion effect comes from the fact that the binding energy between ssDNA and CNT is slightly larger than the CNT–CNT binding, and that the backbone of ssDNA after base–CNT binding is hydrophilic enough to make the ssDNA–CNT complex soluble. The dispersion process depends on the sequence and length of DNA used and, more important, on the CNT diameter and chirality [2]. This demonstration of successful dispersion of CNTs using DNA sequences provides a unique way of separating and sorting CNTs efficiently according to their diameter and electronic properties, which is essential in being able to employ CNTs in practical nanotech-

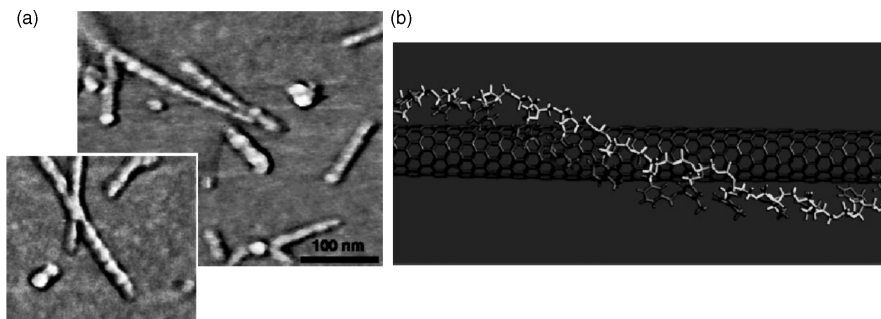


FIGURE 3.5 Helical ssDNA structure wrapping around CNT: (a) AFM images; (b) model from molecular simulations for poly(dT) on CNT(10,0). [(a) Adapted from ref. 2, with permission. Copyright © 2003 American Association for the Advancement of Science. (b) From ref. 1, with permission. Copyright © 2003 Nature Publishing Group.]

nology applications. Computer simulations showed that ssDNA spontaneously wraps into helices from the 3' end to the 5' end, driven by electrostatic and torsional interactions within the sugar–phosphate backbone [36]. We discuss below how even a long genomic ssDNA strand could bind on a CNT, effectively forming a rigid helix whose period is characteristic for the individual DNA–CNT complex [3]. The critical issue in achieving this is removal of the complementary DNA (cDNA) strands from the aqueous solution to assure that all DNA molecules are in single-stranded form. In the same way, ssDNA may disperse CNT bundles into the solution as a whole, without breaking each bundle further into individual CNTs [37].

Double-stranded DNA [4,5] and long RNA homopolymer strands [38] or strands extracted from natural microorganisms [1] could also wrap around CNT effectively. Computer simulations [39] revealed that the hydrophobic end groups, rather than the hydrophilic backbone of the dsDNA, bind on CNTs; the binding mode changes on charged CNTs: The backbone is attracted to a positively charged CNT but there is no dsDNA binding on a negatively charged CNT. By monitoring the shift of peak positions in the optical fluorescence spectrum, a recent study [4] revealed that the dsDNA helix on the CNT gradually switches its configuration from that resembling the B-form of dsDNA to the Z-form, due to the increase in ionic concentration (Figure 3.6).

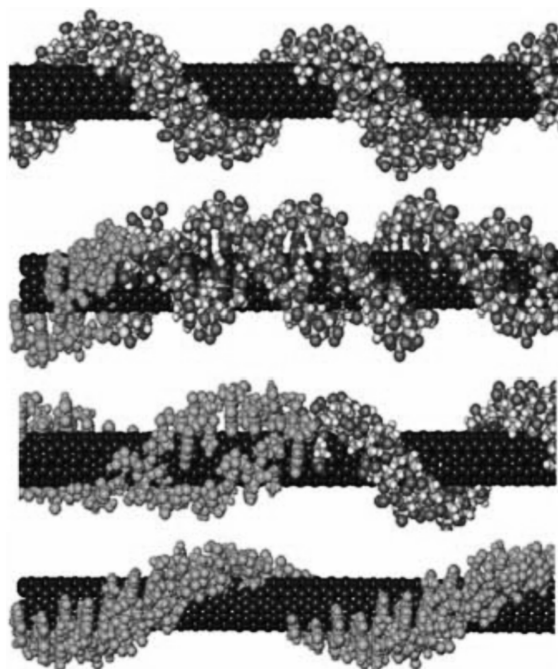


FIGURE 3.6 The dsDNA helix on CNT changes continually from the right-handed B-form to the left-handed Z-form upon the increase of ionic concentration in the solution. (Adapted from ref. 4, with permission. Copyright © 2006 American Association for the Advancement of Science.)

3.2.4 Integration of DNA and a CNT Array

DNA could effectively disperse CNTs into an aqueous solution either as an individual single tube or as bundles [37], where there may be many DNA stands wrapped around the same CNT or the same bundle. On the other hand, it is interesting to consider the possibility of a single DNA molecule binding and connecting several CNTs, in particular a CNT array. The reasons for considering this are: (1) with multiple signal channels, a CNT array could provide a means of sequencing DNA more effectively [12]; and (2) the DNA-connected and assembled CNTs could form useful components of devices for novel electronic applications. A recent study of such a system considered a (10,0) CNT array bound into the major groove of dsDNA [15] (see Figure 3.7). The DNA–CNT interaction reveals effective electronic coupling between the two components, demonstrated by the electronic density distribution of a state 0.7 eV below the highest occupied molecular orbital (HOMO). Interestingly, this contact results in the HOMO state localized exclusively on the CNT and the LUMO (lowest unoccupied molecular orbital) state localized exclusively on the DNA component. A nanoscale electronic switch device, which involves electronic transport in the two perpendicular directions, could be the result of this coupling. Similar contact is also found for the ssDNA as a “molecular wire” connecting a CNT array [12].

3.2.5 DNA Inside CNT Pores

DNA strands could not only bind strongly on the outer surface of CNTs, they could also enter the inner pore of CNTs. The insertion of DNA into nanotubes is interesting because of its relevance to drug delivery and to DNA translocation experiments through nanopores [40], which may be a promising method for DNA detection through

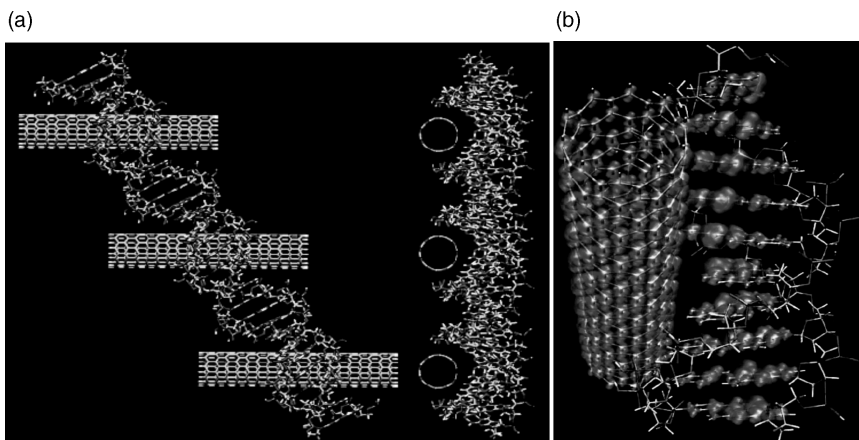


FIGURE 3.7 CNT array in contact with dsDNA: (a) CNTs are incorporated into the major groove of dsDNA; (b) charge density distribution of an electronic state that is 0.7 eV below the HOMO, involving charge distribution on both the DNA and the CNT components.

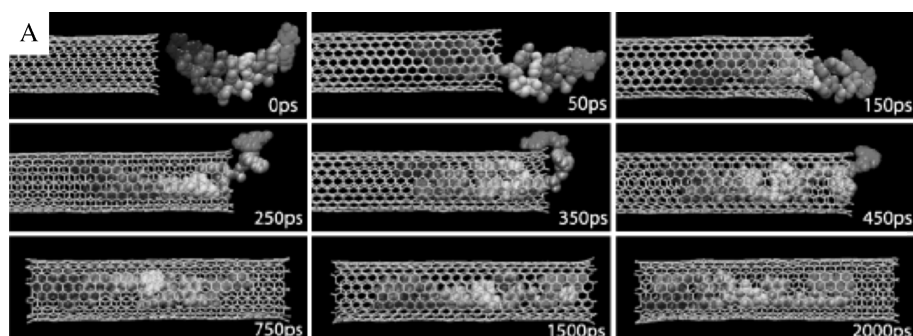


FIGURE 3.8 Insertion dynamics of a ssDNA (dA_8) into the CNT (10,10) from molecular dynamics simulations. (Adapted from *Annual Review of Materials Research*, Vol. 34, p. 123, with permission. Copyright © 2004 Annual Reviews.)

electrical means. DNA insertion into CNT was first considered in MD simulations by Gao et al. [7]. Figure 3.8 shows the dynamics of a ssDNA (8 Å bases) entering a (10,10) nanotube [8]. Initially, CNT and DNA are separated by 6 Å and aligned along the tube axis. The bases start to fill into the nanotube quickly; at time $t = 50$ ps, the first three bases have entered the inner pore of the CNT. The process continues until six out of eight bases fill up the nanotube, at around $t = 200$ ps. The entrance of the last two bases is somewhat hindered during $t = 250$ to 500 ps, due to their interaction with the tube end and the outer surface of CNT. Afterward, the full ssDNA is encapsulated within the inner pore of CNT and reaches the equilibrium state. The van der Waals interaction between the base and the CNT wall is found to be dominant during this insertion process; this is evidenced by the fact that no ssDNA insertion is observed when this interaction is artificially reduced by half. On the other hand, hydrophobic interactions also contribute because polypeptide molecules, which have similar van der Waals interaction with the CNT wall but are less hydrophobic, are hindered in the encapsulation process. The tube size plays a critical role for the DNA insertion: The diameter of the (8,8) CNT (10.8 Å) may be the critical size for ssDNA insertion, below which ssDNA does not enter the CNT pore. The insertion process is also slightly sequence dependent, with purine nucleotides being easier than pyrimidine nucleotides to encapsulate. Finally, double-stranded DNA could also be inserted into the nanotube pores with larger diameters (>27 Å), with the hydrogen bonds between the two complementary strands being partially broken. It was subsequently confirmed by TEM experiments [9] that a DNA strand can indeed be encapsulated into single-walled CNT pores, as observed. The critical issue there is to use radio-frequency and direct-current electric fields for the DNA solution in order to stretch the randomly coiled DNA strands and to irradiate DNA into the CNT coated on the electrode.

Very interestingly, a recent study based on molecular dynamics simulations suggests that the single-stranded RNA molecules can be transported effectively through a transmembrane carbon nanotube (14,14) within a few nanoseconds [41]. The realistic system comprises bare or edge-decorated nanotubes embedded into a dodecane membrane or a lipid bilayer in the aqueous solution. The RNA transport

undergoes repeated stacking and unstacking processes, due to the influence of the steric interaction with the head groups of membrane molecules and the hydrophobic CNT wall. Inside the CNT pore, the RNA structure is reorganized with its backbone solved by water near the CNT axis and its bases aligned with the CNT inner wall.

3.3 ELECTRONIC STRUCTURE

3.3.1 Polarization and Charge Transfer

An essential aspect of the DNA–CNT interaction, and a cornerstone of ultrafast DNA sequencing approaches based on such a combined system, is the electronic structure of its components. The electronic properties of the DNA–CNT can be studied through first-principles quantum mechanical calculations at the single-nucleotide level [24,42]. The interaction between nucleosides and a CNT is illustrated in Figure 3.9(A): In this figure, the density isosurfaces of the charge density difference upon adsorption of nucleoside *A* on the CNT is shown as a representative example of the CNT–nucleoside interaction. The interaction mainly involves the π orbitals of the base atoms, especially the NH_2 group at its end and of the carbon atoms in the CNT. The sugar group of the nucleoside, on the other hand, shows little perturbation in its electronic cloud, mainly in the region proximate to the CNT.

The mutual polarization of π orbitals in the DNA base and the CNT is more obvious in the planar-averaged charge density along the normal to the base plane, shown in Figure 3.9(B). Upon adsorption, the base plane of adenine is positively charged with electron accumulation (near the base) and depletion (near the CNT) in the region between the two components. Integrating this one-dimensional charge distribution in the base and the CNT region, respectively, reveals a net charge transfer of $0.017e$ from *A* to CNT, assuming that the two components are partitioned by the zero difference-density plane close to the CNT wall. This net charge transfer of $0.017e$ from the base to the CNT is rather small compared to that for a typical chemical bond, but is consistent with the weak van der Waals type of interaction between nucleosides and the CNT in this physisorbed system. Moreover, small though it is, this net charge transfer may produce an enhanced sensitivity in the CNT walls for the detection of molecules attached to it, through measuring, for instance, the shift of Raman peaks in the CNT vibrational modes [43].

A detailed analysis of the contributions to the total energy of the system reveals that the attraction between the nucleoside and the CNT is due to exchange–correlation (XC) interactions. Figure 3.10 shows the total energy and the decomposed XC energy and kinetic energy of Kohn–Sham particles as functions of the distance between the DNA base *A* and the CNT wall. We find that the total energy has a minimum at $d = 3.0 \text{ \AA}$, where the XC energy is negative and the kinetic energy is positive, indicating that the nucleoside–CNT attraction arises from XC effects. Beyond the equilibrium distance, the kinetic energy is lowered and has a minimum at $d = 3.75 \text{ \AA}$, while the XC energy keeps increasing and even becomes repulsive in the range $d = 4$ to 5.5 \AA . Similar results were found for *A* adsorbed on graphite [29] and on Cu(110) [44].

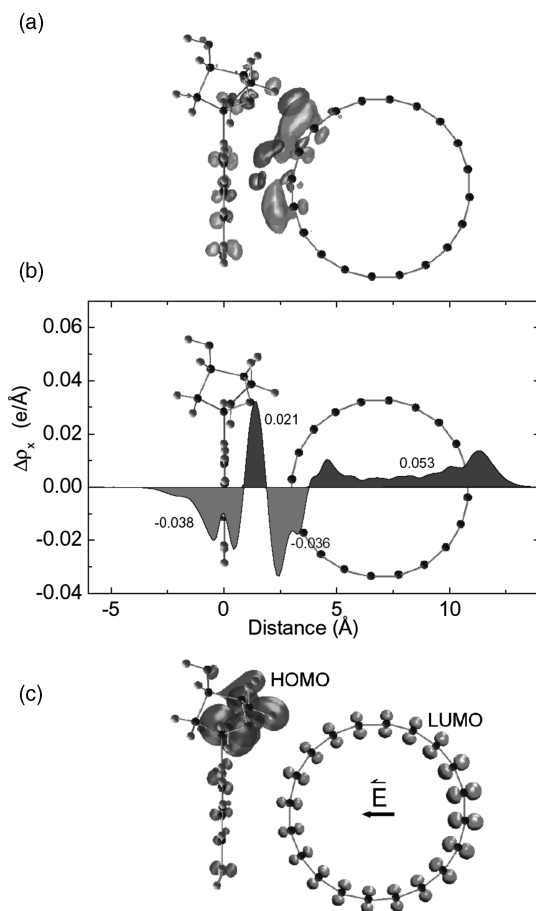


FIGURE 3.9 (a) Isosurfaces of the charge-density difference at levels of $\pm 0.002 e/\text{\AA}^3$ in superposition to the atomic structure for A-nucleoside on CNT. The charge-density difference is obtained by subtracting the charge density of the individual A-nucleoside and CNT systems, each fixed at their respective configurations when they are part of the A/CNT complex, from the total charge density of the A/CNT combined system: $\Delta\rho = \rho[A/CNT] - \rho[A] - \rho[CNT]$, where ρ is the charge density. Electron accumulation and depletion regions are shown in black and gray, respectively. (b) Planar-averaged charge density along the normal direction to the base plane, illustrating the mutual polarization of π orbitals. (c) Isosurface of the density of the HOMO and LUMO states of the combined A/CNT system in the presence of an external electric field of $+0.5 \text{ V/\AA}$.

In electric measurements of the DNA–CNT system, a gate voltage is usually applied to control the conductance [16], while the STM tip itself introduces a field on the order of 0.1 V/\AA . It is therefore interesting to investigate the response of the CNT–DNA system to the applied electric field. We studied this effect by treating the field as a planar dipole layer in the middle of the vacuum region. The external field affects the interaction energy significantly, which depends sensitively on the polarity,

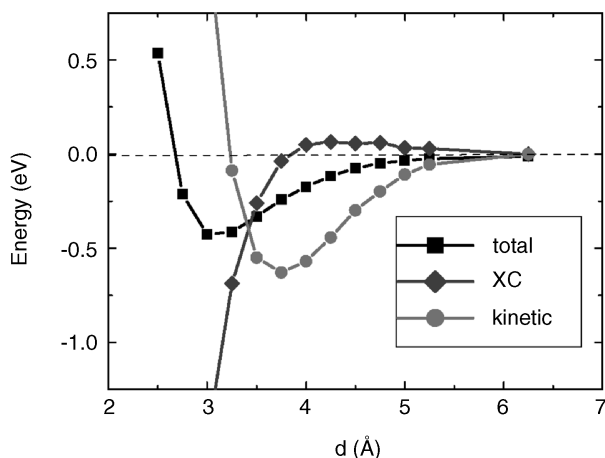


FIGURE 3.10 Relative total energy, decomposed exchange–correlation (XC) energy, and kinetic energy of Kohn–Sham orbits as functions of the base–CNT distance (d) for the DNA base A adsorption on CNT (10,0).

while it leaves almost unchanged the structural features of the system. Taking A–CNT as an example, we find that although a negative field $E_{\text{ext}} = -0.5 \text{ V/\AA}$ (which corresponds to the CNT being negatively charged) hardly changes the adsorption energy (0.436 eV), this energy increases significantly to 0.621, 0.928, and 1.817 eV under external fields of $E_{\text{ext}} = +0.25$, $+0.5$, and $+1.0 \text{ V/\AA}$ (corresponding to the CNT being positively charged). Here the adsorption energy is defined as the energy difference between the total system under E_{ext} with respect to the energy of the CNT under E_{ext} and the free nucleoside. The increase in binding energy under positive electric field is due to the fact that a positive field facilitates the polarization and charge transfer from the base to the CNT. The base–CNT distance, on the other hand, changes only slightly: it is 0.04 Å larger than the zero field value for $E_{\text{ext}} = -0.5 \text{ V/\AA}$ and 0.04 Å smaller for $E_{\text{ext}} = +1.0 \text{ V/\AA}$, respectively. The most prominent change in structure comes from the angle that the NH_2 group at the end of the base makes with the base plane [Figure 3.9(C)]. This angle changes from -27° at $E_{\text{ext}} = -0.5 \text{ V/\AA}$ to $+25^\circ$ at $E_{\text{ext}} = +1.0 \text{ V/\AA}$, indicating the softness of the C– NH_2 bond. The configuration under positive field resembles that on Cu(110) [44]. Other nucleosides have the same behavior given their similarity in structure. Therefore, the applied electric field stabilizes the DNA bases on the CNT without disturbing the zero-field adsorption geometry. The more profound effect of the electric field lies in the change of electronic structure; for instance, the HOMO and LUMO become spatially separated under an external field of $E_{\text{ext}} = +0.5 \text{ V/\AA}$, with the first localized on the nucleoside A and the second on the CNT, as indicated in Figure 3.9(C).

We have discussed in some detail the DNA–CNT interaction at the single-base level. In reality, when a DNA strand comes into close contact with a CNT, the interaction between them can be approximated as the superposition of the interactions of individual base–CNT units, which depends on the base identity. This is exemplified

by the overlap of charge distribution on both components in the dsDNA–CNT structure in Figure 3.7. The polarizability of the combined DNA–CNT system might be screened by the bound DNA strand, depending on the DNA density and geometry and on the nanotube diameter and chirality. We expect that thermal fluctuations of counterions and water will average out to a zero net contribution to the local field around the DNA–CNT system.

3.3.2 Density of States

The electronic density of states (DOS) describes the energy-level distribution of electrons and is a quantity directly accessible to experimental measurements: for example, through the differential current–voltage (dI/dV) in scanning tunneling spectroscopy (Figure 3.1). The characteristic features of the electronic structure for single DNA nucleoside adsorption on CNT is shown in the DOS plot of Figure 3.1(b) and in more detail in Figure 3.11. In Figure 3.1(b), the DOS peaks for the combined nucleoside–CNT system differ significantly from those of the bare CNT. The energy gap calculated for the CNT is 0.8 eV [45]. The difference in DOS between the bare CNT and the combined CNT–nucleoside system [Δ DOS, red curve in Figure 3.1(b) and all curves in Figure 3.11(A) and (B)] has features that extend through the entire range of energies; those close to the Fermi level are the most relevant for our discussion. These features can serve as the signal to identify DNA bases in current–voltage measurements or photoelectron spectroscopy. This “electronic fingerprint” is independent of the relative orientation of the nucleoside and the CNT, as shown in Figure 3.11; the Δ DOS for the three to four dominant configurations of the four nucleosides on CNT have essentially the same features. However, the Δ DOS peaks for *different* bases differ significantly from each other, which is encouraging as far as base identification is concerned. In Figure 3.11(C) and (D) we show the positions of the first peak below and above the Fermi level in the Δ DOS plots for A, C, G, and T adsorbed on the CNT. These two peaks correspond to the HOMO and LUMO of the bases, respectively. The spatial distribution of the corresponding wavefunctions for all four DNA bases is shown in Figure 3.12. We found that in the DOS plots of Figure 3.11(A) and (B), the HOMO and LUMO positions of the different bases are clearly distinguishable, while for a given base, the different adsorption geometries produce essentially indistinguishable peaks.

When a gate voltage is applied, the HOMO and LUMO peaks of the bases shift continuously with respect to the CNT DOS features. The latter change little under small gate voltage or electric field. For example, the bandgap of the CNT shrinks by only 0.03 eV for a field of $E_{\text{ext}} = 0.5 \text{ V/\AA}$ relative to its zero-field value. As is evident from Figure 3.11(C) and (D), it is possible to induce a shift of the DNA base peaks relative to the CNT features with external voltage so as to facilitate experimental measurements. The CNT HOMO and LUMO orbitals serve as a definitive, easily distinguishable reference in evaluating DOS features of the adsorbed DNA nucleosides. The HOMO and LUMO peaks of all DNA bases shift monotonically with applied external field, by about 0.7 eV for $E_{\text{ext}} = 0.25 \text{ V/\AA}$. Interestingly, when the external field is sufficiently large, the HOMO of all four bases falls within the bandgap

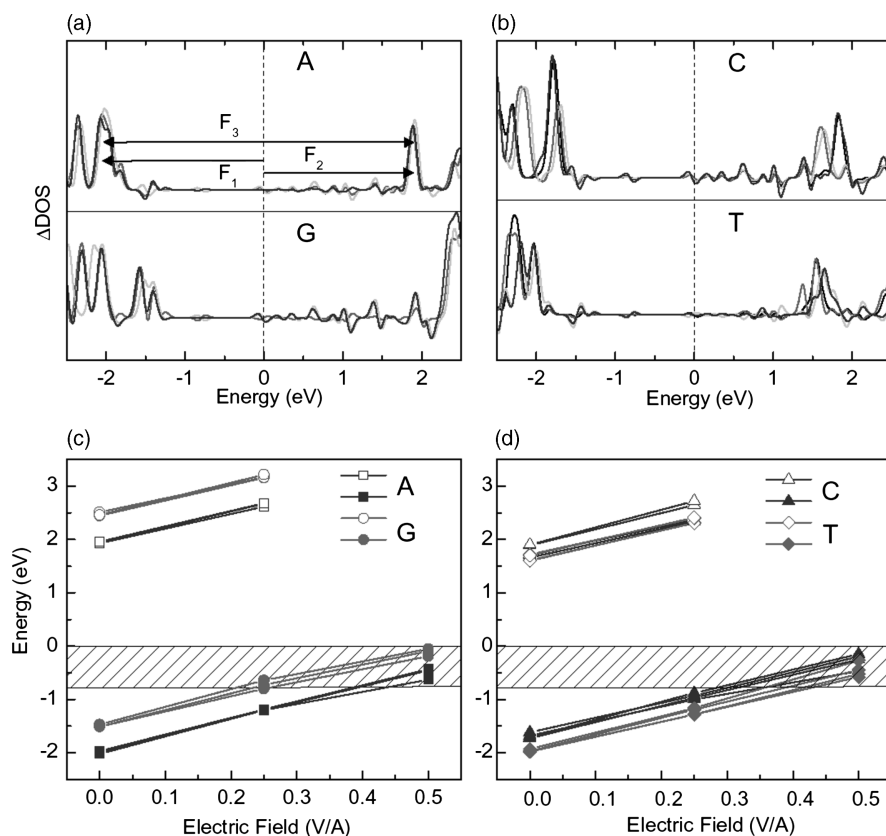


FIGURE 3.11 Density of states. (a), (b) DOS difference, Δ DOS, for the dominant nucleoside configurations on the nanotube. The zero of the energy scale is set to the conduction band minimum of the CNT. The features F_1 , F_2 , and F_3 energy separations between different orbitals, are identified. (c), (d) Variation of the HOMO energy level (open symbols) and the LUMO energy level (open symbols) of the four nucleosides on CNT, as a function of the magnitude of applied electric field. The shaded area is the energy gap of the CNT.

of the CNT [Figure 3.11(C) and (D)], which should enhance the sensitivity of experimental measurements to the type of base. At the highest field we studied, $E_{\text{ext}} = 0.5 \text{ V/\AA}$, the bandgap of the combined CNT–DNA systems is 0.51 eV for A, 0.45 eV for T, 0.27 eV for C, and 0.11 eV for G, on average, sufficiently different from each other to be clearly distinguished.

3.3.3 STM Images

For a direct real-space identification of DNA bases on CNT, a scanning tunneling microscopy (STM) image would be useful. We have simulated the STM images based on the Tersoff–Hamann theory [46]. The STM images in Figure 3.13 correspond to an

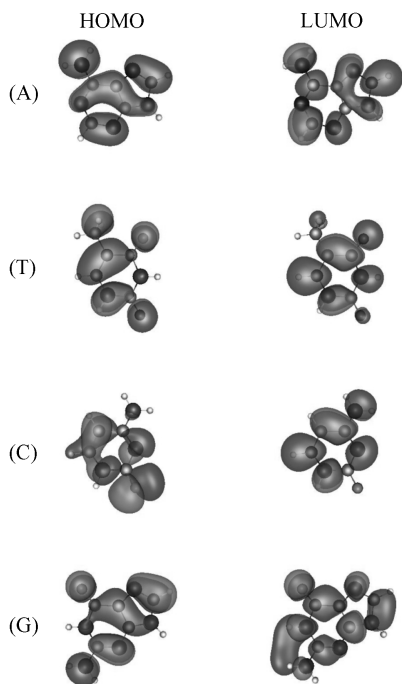


FIGURE 3.12 Wavefunctions of the HOMO and LUMO states for the four DNA bases. Black and gray clouds indicate positive and negative values.

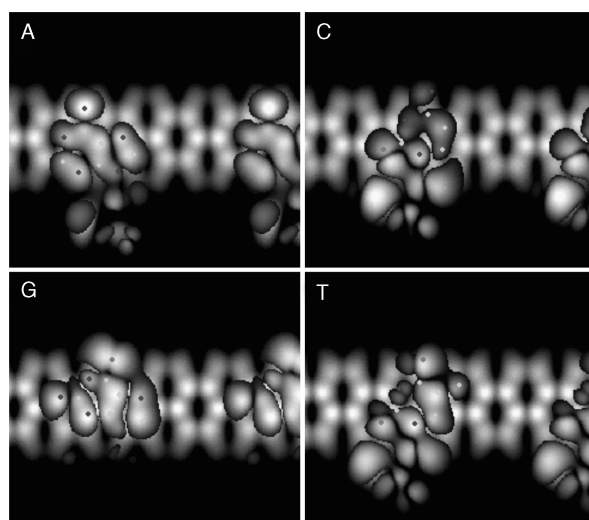


FIGURE 3.13 Simulated STM images of DNA bases on the (10,0) CNT. Small dots indicate the positions of the heavy atoms in the bases (light gray for C, black for N, and dark gray for O).

applied voltage of +1.4 V, which integrates the charge densities of states within the energy range -1.4 to 0 eV below the HOMO (including HOMO). It is clear that the STM images for the four DNA nucleoside have different spatial characteristics, which, with sufficient image resolution, could provide identification of the four bases directly. The STM images have a correspondence to the wavefunctions of DNA bases shown in Figure 3.12, as long as the energies of those states fall in the correct range of -1.4 to 0 V below the HOMO of the CNT.

3.4 OPTICAL PROPERTIES

The combination of DNA and CNT structures exhibits interesting optical properties that are accessible by standard optical measurements, including Raman, infrared–visible–ultraviolet (UV) absorption, dichroism, and fluorescence spectroscopy. The advantage is that as CNTs show rich and characteristic optical signatures, the changes in these easily measurable optical signals resulting from the presence of DNA strands wrapped around the CNT could be used as an identifier for the attached DNA strand. It would be helpful if these changes are sequence dependent and if they were sensitive at the single-base level. If the level of sensitivity can be established, these considerations suggest the development of novel DNA detection and sequencing methods based on optical signals.

The simplest system for addressing this issue is a DNA homopolymer wrapped around a CNT. Hughes et al. [47] have recently measured the UV–visible absorption of ssDNA homopolymers consisting of about 30 bases wrapped around CNTs in aqueous solution. Different DNA homopolymers show significant differences in optical absorption (both magnitude and peak positions) in the ultraviolet range 200 to 300 nm. The difference between absorption by the DNA–CNT combined system and the isolated, bare CNT, which constitutes the absorption signature of the DNA strand attached to the CNT wall, is shown in Figure 3.14 for the DNA homopolymers poly(dA), poly(dC), poly(dG), and poly(dT). There are significant differences from case to case in terms of absorption peak positions and their relative intensity. For instance, there are two peaks for A, at 266 and 213 nm, with the second having twice the intensity of the first; there are also two peaks, at 275 and 204 nm, for C, with the first peak showing higher intensity.

In the experimental measurements, there are significant changes in the spectrum of DNA on the CNT compared with that of free ssDNA in solution. For example, the first peak, centered at 260 nm, for free poly(dA) is red-shifted to 266 nm when A is adsorbed on CNT, and the peak at 203 nm is shifted to 213 nm. Similar changes are found in the various spectra of the other three bases. For poly(dC), the broad peak at 230 to 250 nm diminishes, the peak at 200 nm is reduced by half, while the peak at the longest wavelength (310 nm) does not change. For G, the peak at 275 nm remains constant while the peak at 248 nm is reduced by half and the peak at 200 nm increases slightly after adsorption on CNT. For T, there is no apparent change for the peak at 270 nm, while the adsorption in the range 210 to 240 nm is reduced significantly. The origin for these spectrum changes on DNA binding on CNT must be related to

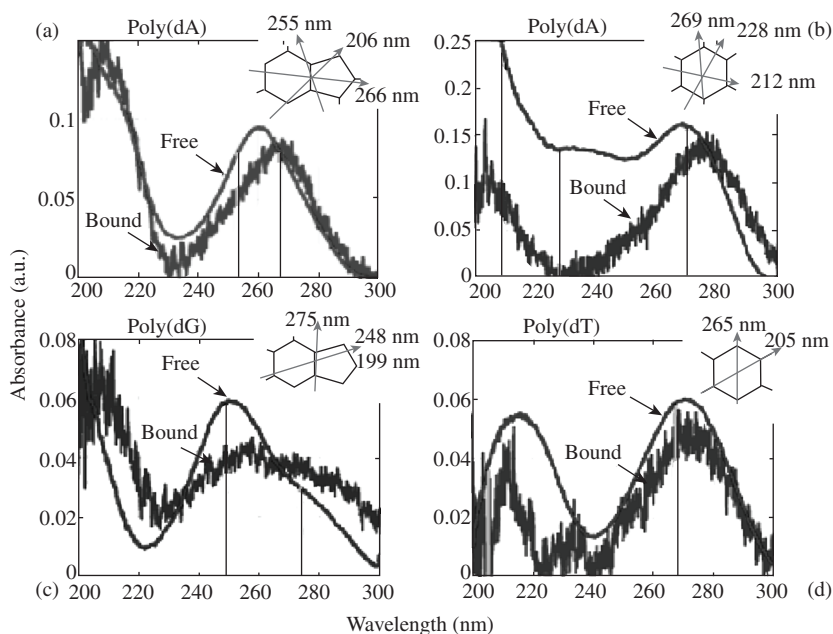


FIGURE 3.14 Optical adsorption of ssDNA homopolymer on CNT (thick lines) and in free solution (thin lines). (From ref. 47, with permission. Copyright © 2007 American Chemical Society.)

corresponding changes in electronic structure, which can be elucidated only through detailed theoretical calculations.

To address this issue, we have calculated orientation-dependent absorption spectra of DNA bases adsorbed on single-walled CNTs [48], as shown in Figure 3.15. We compare the spectrum of the DNA base along each polarization direction of incident light (the direction of the electric field vector) with the spectrum measured experimentally for the combined ssDNA–CNT systems. From these comparisons, all the features described above can be reproduced accurately in our calculations by considering the absorption of the base along a certain light-polarization direction only. CNTs have a dominant, intrinsic, and diameter-independent absorption peak in the ultraviolet region at 236 nm with polarization perpendicular to their axis [49]. Therefore, only photons with polarization parallel to the CNT axis are available to interact with the attached DNA bases, or equivalently, the nanotube produces a local electric field aligned along its axis (the *hypochroism effect*). This explains why the absorption spectra of the DNA bases change when they are attached to the nanotube wall: The direction of tube axis is indeed the preferred direction for UV absorption by the bases.

Consequently, the agreement of the calculated changes in absorption with the experimental results strongly suggests that there is a preferred absorption direction for the bases on the CNT, a desirable feature favoring ultrafast DNA sequencing based on optical properties of this system. This result is further supported by the comparison

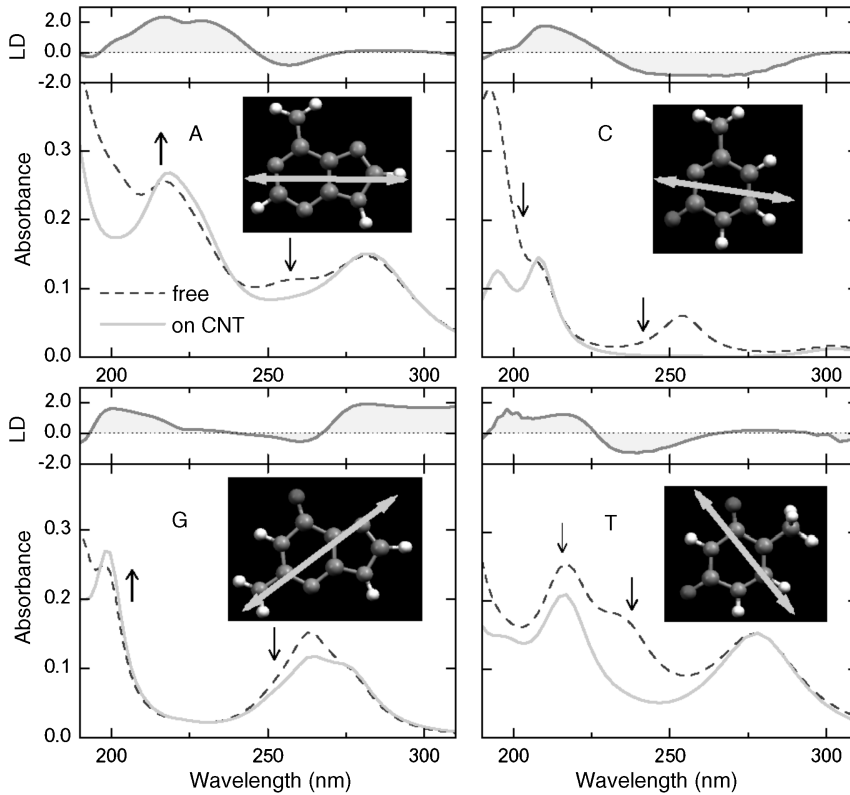


FIGURE 3.15 Absorption spectrum of DNA bases averaged over all field directions (dashed lines) and along a particular direction (indicated by double-headed arrows in the insets) that mimics the nanotube axis (solid line). These spectra reproduce adequately the experimentally measured spectra in solution. Vertical arrows indicate intensity changes in experimental spectra after base adsorption on the CNT. Linear dichroism spectra that best match experiment are also shown on top of each panel.

between the calculated linear dichroism curves and the measured ones [50]. In the inserts of Figure 3.15 the lines show the direction of the CNT axis along which the experimental absorbance spectra of ssDNA wrapped on CNTs are best reproduced. The orientations of the nanotube axis relative to the bases as determined from this approach agree well with the global energy-minimum structures from force-field calculations, the only exception being T. Specifically, the directions of the nanotube axis from absorbance spectra, linear dichroism, and structural optimization are: 89° , 105° , 98° for A; -100° , -84° , -90° for C; -58° , -30° , -61° for G; and 39° , 40° , 75° for T. Overall, the agreement between experiment and theory is very reasonable given the complicated nature of both the experimental measurements and theoretical results. This provides a way to determine the base orientation relative to the nanotube axis in the DNA–CNT system from the optical absorption data.

Besides determining the base orientations, the optical spectra of the DNA–CNT systems are also used for identifying the types of enriched CNTs [2], sensing sugar in solutions [5], detecting DNA hybridization [17], and monitoring morphology changes of DNA on CNTs [4], as discussed in more detail below.

3.5 BIOSENSING AND SEQUENCING OF DNA USING CNTs

3.5.1 Gaseous Sensing Using DNA–CNT

One of the most successful applications of DNA–CNT systems has been the detection of chemical substances [51]. In such applications, the presence of certain molecules can be converted into electric signals: DNA is used as the chemical recognition site and single-walled CNT field-effect transistors (FETs) as the electronic readout unit. The fundamental principles here are that CNTs, as either a metallic system or a narrow bandgap semiconductor, can conduct electricity and be used in a FET, and that the conductivity of CNTs is strongly influenced by the presence of functional groups, either covalently bound to the CNT walls or ends, or physically adsorbed on the CNT wall, especially wrapped DNA. Gaseous molecules or other chemicals induce a change in the configuration or electronic structure of the bound DNA, due to its large structural variability, which in turn results in a change in the conductivity of the CNT–FET. We discuss next two specific applications of this type.

Figure 3.16(a) shows schematically the device setup made of ssDNA–CNT [14]. The chemical formula of some ordinary gases to be detected is shown in (b), and results are demonstrated in Figure 3.16(c)–(e). Due to its chemically inert nature, the bare CNT is not sensitive enough to have a detectable conductivity change when the gas odors of propionic acid, trimethylamine, and methanol are passing through the device channels. The situation changes, however, for the ssDNA-decorated CNTs, which exhibit a sensitive interaction between the gases and the ssDNA on the CNT. Conductivity changes due to the various gas odors differ in sign and in magnitude, and can be tuned by choosing different DNA base sequences. For example, propionic acid and methanol give positive (increase) and negative changes (decrease) in electric conductivity of the CNT wrapped with a ssDNA sequence of 5′GAGTCTGTGGAGGAGGTAGTC3′ [Figure 3.16(e)], making this ssDNA–CNT structure a sensitive detector. The sensing device is robust and sustains at least 50 gas exposure cycles. It is rapid in response and recovers in seconds in airflow. All these attributes make this device promising as an electronic “nose” or “tongue” for molecular detection, disease diagnosis, and home security applications. Recently, a counterpart DNA–CNT device for detecting glucose in a biology-relevant environment in the presence of the glucose oxidase enzyme was developed [5].

3.5.2 Field-Effect Transistor and Optical Shift for DNA Detection

An even more challenging issue is the detection of DNA strands using bare or DNA-decorated CNTs. There are, however, some successful examples of DNA detection

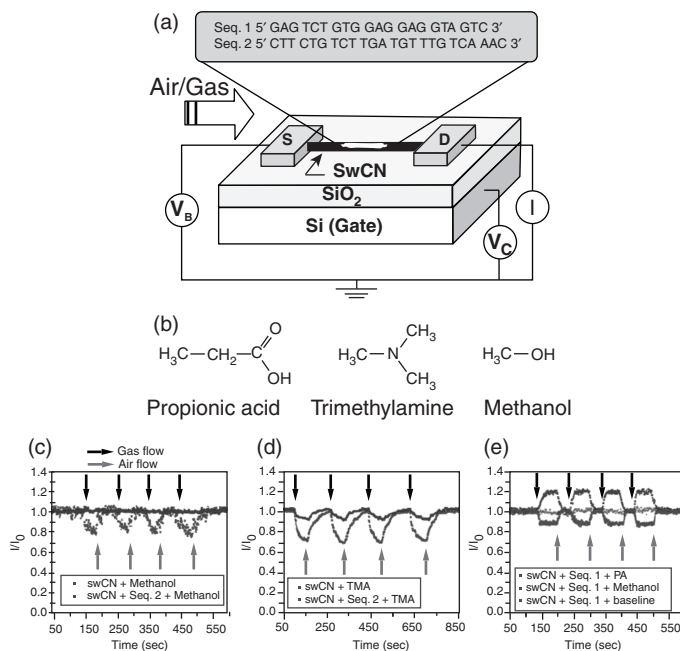


FIGURE 3.16 ssDNA-CNT as a chemical sensor: (a) device setup; (b) molecules to be detected; (c–e) responses in conductivity to gaseous flows and recovery in air using bare and DNA-decorated CNTs. Two different ssDNA sequences are employed as shown in (a). PA, propionic acid; TMA, trimethylamine. (Adapted from *Nano Letters*, Vol. 5, p. 1174, with permission. Copyright © 2005 American Chemical Society.)

using devices made of ssDNA–CNT, through either electric [12,16] or optical means [17]. For instance, the source–drain conductance measurement of the CNT FET device shows a large shift (decrease) in conductivity for the bare and the ssDNA-wrapped CNTs [16]. The conductivity is lowered further in the presence of other DNA strands; the complementary strand (cDNA) to that incubated onto the CNTs shows the largest reduction in conductance, while a noncomplementary strand (ncDNA) shows fewer pronounced changes or no change at all. This conductivity drop also depends sensitively on the concentration of ssDNA in solution at picomolar to micromolar levels. Therefore, this simple device could be used effectively for label-free detection of the cDNA and its concentration. This method has been demonstrated to have a sensitivity at the level of single-nucleotide mismatch between the two strands. The sensitive dependence of signals on the counterion concentration suggests that the reduction in conductivity upon ssDNA immobilization and hybridization relies on the screening effect of charges around the CNT from the added ssDNA.

The same idea was demonstrated for the detection of DNA hybridization through bandgap fluorescence measurements of the CNTs [17]. The addition of cDNA in the ssDNA-wrapped CNT solution resulted in a 2-meV increase in the emission energy of bandgap fluorescence peak of the nanotube, whereas for a ncDNA strand there is little

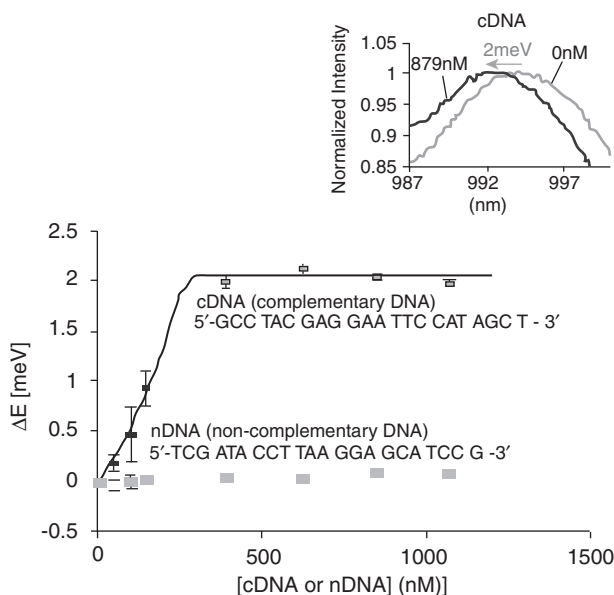


FIGURE 3.17 Optical DNA detection. Addition of complementary DNA (cDNA) strand to the ssDNA-wrapped CNT solution causes an energy increase in the CNT bandgap fluorescence peak, while there is no detectable change for adding noncomplementary strands. The peak shift is dependent on the cDNA concentration. Insert: sample spectra showing a blue shift in the fluorescence peak with cDNA addition. (From ref. 17, with permission. Copyright © 2006 American Chemical Society.)

or no shift (Figure 3.17). Again, this shift of the peak depends almost linearly on the concentration of cDNA from 1 to 400 nM. The energy shift observed in experiments can be interpreted as an increase in the exciton binding energy due to the increased surface area of the CNT covered by ssDNA upon hybridization. This energy shift in the CNT bandgap fluorescence provides an easy way to detect cDNA in solution and to monitor the DNA hybridization process by an optical means. Electronic or optical DNA detection using ssDNA-decorated CNTs has the advantages of being label-free, low cost, highly sensitive, simple, and of high accuracy, and represents an important step toward practical molecular diagnostics.

3.5.3 Monitoring Morphology Changes of dsDNA

As mentioned earlier, the change of the dsDNA from the right-handed B-like form to the left-handed Z-like form can also be monitored by measuring the optical responses (fluorescence and circular dichroism) of DNA strands on a (6,5) CNT (Figure 3.6), as a response to the increase in divalent metal cation concentration [4]. The assumption is that the surface area of CNT covered by dsDNA increases during the transition from the B to the Z form; thus, the exciton-binding energy of the CNT increases. This is

interesting because it provides an inexpensive way to detect molecular structures in the NANO–BIO hybrid complex at the nanoscale.

3.5.4 DNA Sequencing

All methods discussed so far measure the effects of a DNA strand as a whole. They are very useful for detection of DNA strands, but in terms of DNA sequencing, one has to go a step further and determine explicitly the effect on CNT properties of changes in electronic or optical signals corresponding to a *single nucleotide*. We discussed in Section 3.3 the fact that the four nucleosides introduce characteristic peaks in the density of states of the DNA–CNT complex, which points to the possibility of employing these characteristics for DNA single-base detection and DNA sequencing. The setup we envisaged for this purpose is shown in Figure 3.1: A fragment of ssDNA is brought into close contact with the CNT and wraps around it partially. A force can be exerted on one end of the DNA: for example, by attaching to a bead that can be manipulated by optical [52] or magnetic means [53]. This will lead to a situation in which a few (even a single) base is in intimate contact with the CNT. By pulling the ssDNA fragment, the bases along it will interact successively with the CNT, allowing for measurements of the interaction. A setup in which the CNT can rotate in synchronization with the DNA pulling process may facilitate the motion.

Inspired by the calculations of the DOS of the nucleoside–CNT complex, the present authors and collaborators have proposed measuring the electronic structure to identify bases by a probe sensitive to local electronic states, such as scanning tunneling spectroscopy, using a stationary STM tip in the geometry similar to that described by Kong et al. [54]. This type of method has a high resolution of about 2 Å and is used routinely to investigate the local electronic structure of adsorbates on semiconductor surfaces. For example, local density of states of aniline ($C_6H_5NH_2$) on Si(100) was clearly measured [55]. To maximize the sensitivity of such measurements, it is desirable to have a semiconducting CNT as the substrate. Such a setup also overcomes the difficulty in the older proposals of distinguishing DNA bases by measuring the transverse conductance of an electrode–ssDNA–electrode junction, where it was found that transverse conductance cannot be used to distinguish nucleotides because ssDNA is too flexible when in the neighborhood of the electrode [21]. In our case the DNA bases are bound on the CNT at a constant distance of 3.4 Å from the CNT wall and with a definitive orientation, as we have shown in Sections 3.2 and 3.4, forming a very stable and robust DNA–CNT complex, which would constrain the DNA–electrode geometry in a desired, well-controlled manner. The device proposed in Figure 3.1 serves only as an idealized case in point to illustrate the key concepts. We note that there may exist several equivalent experimental setups toward the same goal. For instance, sequentially embedding the ssDNA–CNT structure into a nanopore and measuring the transverse conductance from the CNT to the nanopore wall could be an equally promising approach.

To test the validity of the proposed detection of DNA bases, we evaluated the efficiency of base identification using data generated from the Δ DOS calculations as

input to a neural network classifier, which was trained to produce as output the label of the DNA base (A, C, G, or T). Specifically, we extracted six simple representative features (F_i , $i = 1$ to 6) in an energy window from -3 to 3 eV around the Fermi level:

- F_1 : location of the base HOMO
- F_2 : location of the base LUMO
- F_3 : bandgap of the base (LUMO–HOMO distance)
- F_4 : number of prominent peaks below the Fermi level
- F_5 : location of the highest occupied peak
- F_6 : integral of the occupied states from -3 to 3 eV

Features F_1 , F_2 , and F_3 are indicated in Figure 3.11 for A/CNT. We produced a robust scheme for identifying the bases by employing artificial neural networks [56] and find that the network can deliver 100% efficiency even after taking into consideration the measurement errors (e.g., an error of ± 0.10 eV in energy). For practical applications it is important to evaluate the significance of each feature individually. To this end, we tested the discriminating ability of each of the six features defined and found that the location of base HOMO–LUMO (F_1/F_2) and the HOMO–LUMO gap (F_3) are the most informative features, while the number of occupied states (F_4) and the location of the highest peak (F_5) are less so. The HOMO–LUMO gaps alone, which are 3.93 to 4.02 eV for A, 3.34 to 3.62 eV for C, 3.93 to 4.02 eV for G, and 3.58 to 3.69 eV for T, could easily discriminate A and G from C and T. Certain features are complementary, and combinations of just two features can actually yield 100% efficiency. For instance, if the location of HOMO (-2.02 eV for A, -1.68 eV for C, -1.51 eV for G, and -1.98 eV for T), which is well defined in experiments with respect to the DOS peaks of the CNT, is used in addition to the HOMO–LUMO gap, A is easily discriminated from G (and C from T), resulting in 100% efficiency for the combination of features F_1 to F_3 . The external field magnifies these differences, making the base classification even more robust. With a field of 0.25 eV/Å, several triplets of features produce 100% efficiency in base identification.

3.6 SUMMARY

We have reviewed the fundamental aspects of DNA interaction with CNTs and have discussed the prospects of DNA sensing and sequencing using DNA–CNT complexes. Due to the large variety in structures of the two components, such as different diameters, chiralities, conducting properties, single- or multiwalled CNTs, isolated CNTs or bundles of CNTs, and single- or double-stranded DNA as well as different forms, various lengths, and different sequences, the combined DNA–CNT system exhibits a truly rich variety of artificial nanostructures, for which wide applications can be envisaged. Among them, the most significant might be the robust helical structure formed by wrapping DNA around a CNT, which has characteristic structural and

electronic features, that may enable ultrafast DNA sequencing. To this end, the most important properties of the DNA–CNT complex are:

- Long genomic single-stranded DNA can wrap around a single-walled CNT, forming a tight, stable helix. The lateral periodicity remains constant for any single ssDNA–CNT, but is dependent on the CNT diameter and the DNA sequence.
- The bases in the ssDNA are almost fixed in geometry bound on the CNT. They are stabilized at 3.4 Å away from the CNT wall through mainly van der Waals attraction and the hydrophobic effect. Although a very large number of nonequivalent configurations may be present, only a few of them are dominant. Moreover, each type of base prefers to have a definite orientation with respect to the CNT axis: 90° for A, 80° for C, 120° for G, and 40° for T.
- Because DNA bases are attached rigidly to the CNT, the noise in transverse conductance measurements can be minimized. Our quantum mechanical calculations show that the four types of nucleotides introduce distinct characteristic features in the local density of states. These features are easily recognizable and produce 100% accuracy in our artificial neural network for DNA base identification.

Based on these observations, we suggest that the DNA–CNT system is very promising in terms of DNA detection and DNA sequencing through electronic means, upon which a low-cost, ultrafast, accurate, and largely parallel DNA sequencing method could eventually be built. In addition, this system can be the basis for diverse applications, combining the robustness of CNTs with the flexibility of DNA in a unique building block that blends artificial and natural materials at the nanometer scale.

Acknowledgments

It is a pleasure to acknowledge the numerous original contributions to the work reviewed here by our collaborators: P. Maragakis, G. Lu, C. Papaloukas, and W. L. Wang. The original work was supported in part by grants from the U.S. Department of Energy and the Harvard University Center for the Environment. We are indebted to M. Fyta, M. Hughes, F. Albertorio, J. Golovchenko, and D. Branton for helpful discussions.

REFERENCES

1. Zheng M, Jagota A, Semke ED, et al. DNA-assisted dispersion and separation of carbon nanotubes. *Nat. Mater.* 2003;2:338–342.
2. Zheng M, Jagota A, Strano MS, et al. Structure-based carbon nanotube sorting by sequence-dependent DNA assembly. *Science.* 2003;302:1545–1548.
3. Gigliotti B, Sakizzie B, Bethune DS, Shelby RM, Cha JN. Sequence-independent helical wrapping of single-walled carbon nanotubes by long genomic DNA. *Nano Lett.* 2006;6:159–164.

4. Heller DA, Jeng ES, Yeung TK, et al. Optical detection of DNA conformational polymorphism on single-walled carbon nanotubes. *Science*. 2006;311:508–511.
5. Xu Y, Pehrsson PE, Chen L, Zhang R, Zhao W. Double-stranded DNA single-walled carbon nanotube hybrids for optical hydrogen peroxide and glucose sensing. *J. Phys. Chem. C*. 2007;111:8638–8643.
6. Gladchenko GO, Karachevtsev MV, et al. Interaction of fragmented double-stranded DNA with carbon nanotubes in aqueous solution. *Mol. Phys.* 2006;104:3193–3201.
7. Gao HJ, Kong Y, Cui D, Ozkan CS. Spontaneous insertion of DNA oligonucleotides into carbon nanotubes. *Nano Lett.* 2003;3:471–473.
8. Gao HJ, Kong Y. Simulation of DNA–nanotube interactions. *Annu. Rev. Mater. Res.* 2004;34:123–150.
9. Okada T, Kaneko T, Hatakeyama R, Tohji K. Electrically triggered insertion of single-stranded DNA into single-walled carbon nanotubes. *Chem. Phys. Lett.* 2006;417:288–292.
10. Watson JD, Crick FHC. Molecular structure of nucleic acids: a structure for deoxyribose nucleic acid. *Nature (London)*. 1953;171:737–738.
11. Iijima S. Helical microtubules of graphitic carbon. *Nature (London)*. 1991;354:56–58.
12. Li J, Ng HT, Cassell A, et al. Carbon nanotube nanoelectrode array for ultrasensitive DNA detection. *Nano Lett.* 2003;3:597–602.
13. Kam NWS, Liu ZA, Dai HJ. Carbon nanotubes as intracellular transporters for proteins and DNA: an investigation of the uptake mechanism and pathway. *Angew. Chem. Int. Ed.* 2006;45:577–581.
14. Staii C, Johnson AT, Chen M, Gelperin A. DNA-decorated carbon nanotubes for chemical sensing. *Nano Lett.* 2005;5:1774–1778.
15. Lu G, Maragakis P, Kaxiras E. Carbon nanotube interaction with DNA. *Nano Lett.* 2005;5:897–900.
16. Star A, Tu E, Niemann J, Gabriel JP, Joiner CS, Valcke C. Label-free detection of DNA hybridization using carbon nanotube network field-effect transistors. *Proc. Natl. Acad. Sci. USA*. 2006;103:921–926.
17. Jeng ES, Moll AE, Roy AC, Gastala JB, Strano MS. Detection of DNA hybridization using the near-infrared band-gap fluorescence of single-walled carbon nanotubes. *Nano Lett.* 2006;6:371–375.
18. Nakashima N, OKuzono S, Murakami H, Nakai T, Yoshikawa K. DNA dissolves single-walled carbon nanotubes in water. *Chem. Lett.* 2003;32:456–457.
19. Takahashi H, Numao S, Bandow S, Iijima S. AFM imaging of wrapped multiwall carbon nanotube in DNA. *Chem. Phys. Lett.* 2006;418:535–539.
20. Lu Y, Bangsaruntip S, Wang X, Zhang L, Nishi Y, Dai HJ. DNA functionalization of carbon nanotubes for ultrathin atomic layer deposition of high kappa dielectrics for nanotube transistors with 60 mV/decade switching. *J. Am. Chem. Soc.* 2006;128:3518–3519.
21. Zhan XG, Krstic PS, Zikic R, Wells JC, Fuentes-Cabrera M. First-principles transversal DNA conductance deconstructed. *Biophys. J.* 2006;91:L4–L6.
22. Zwolak M, Di Ventra M. Electronic signature of DNA nucleotides via transverse transport. *Nano Lett.* 2005;5:421–424.
23. Lagerqvist J, Zwolak M, Di Ventra M. Fast DNA sequencing via transverse electronic transport. *Nano Lett.* 2006;6:779–782.

24. Meng S, Maragakis P, Papaloukas C, Kaxiras E. DNA nucleoside interaction and identification with carbon nanotubes. *Nano Lett.* 2007;7:45–50.
25. Brooks BR, Bruccoleri RE, Olafson BD, States DJ, Swaminathan S, Karplus M. CHARMM: a program for macromolecular energy, minimization, and dynamics calculations. *J. Comp. Chem.* 1983;4:187–217.
26. MacKerell AD Jr., Bashford D, Bellott RL, et al. All-atom empirical potential for molecular modeling and dynamics studies of proteins. *J. Phys. Chem. B.* 1998;102:3586–3616.
27. Krivov SV, Chekmarev SF, Karplus M. Potential energy surfaces and conformational transitions in biomolecules: a successive confinement approach applied to a solvated tetrapeptide. *Phys. Rev. Lett.* 2002;88:038101.
28. (a) Elber R, Karplus M. Multiple conformational states of proteins: a molecular-dynamics analysis of myoglobin. *Science* 1987;235:318–321. (b) Wales DJ, Scheraga HA. Review: Chemistry—global optimization of clusters, crystals, and biomolecules. *Science* 1999;285:1368–1372. (c) Wales DJ. A microscopic basis for the global appearance of energy landscapes. *Science* 2001;293:2067–2070.
29. Ortmann F, Schmidt WG, Bechstedt F. Attracted by long-range electron correlation: adenine on graphite. *Phys. Rev. Lett.* 2005;95:186101.
30. Gowtham S, Scheicher RH, Ahuja R, Pandey R, Karna SP. Physisorption of nucleobases on graphene: density-functional calculations. *Phys. Rev. B.* 2007;76:033401.
31. For these calculations we employed a periodic supercell with dimensions of $20 \text{ \AA} \times 20 \text{ \AA} \times 12.78 \text{ \AA}$. Larger supercells show minor differences in the structural and electronic features: a sampling of a $1 \times 1 \times 3$ k -point mesh in reciprocal space is used to generate the charge density and the density of states. Gaussian smearing of electronic eigenvalues with a width of 0.1 eV is employed.
32. Freund JE. Ph.D. dissertation. Ludwig-Maximilians Universität München, 1998.
33. Jorgensen WL, Chandrasekhar J, Madura JD, Impey RW, Klein ML. Comparison of simple potential functions for simulating liquid water. *J. Chem. Phys.* 1983;79:926–935.
34. Berendsen HJC, Postma JPM, Nola AD, Haak JR. Molecular-dynamics with coupling to an external bath. *J. Chem. Phys.* 1984;81:3684–3690.
35. Darden T, York D, Pedersen L. Particle mesh Ewald: an $N \log(N)$ method for Ewald sums in large systems. *J. Chem. Phys.* 1993;98:10089–10092.
36. Johnson RR, Johnson ATC, Klein ML. Probing the structure of DNA–carbon nanotube hybrids with molecular dynamics. *Nano Lett.* 2008;8:69–75.
37. Cathcart H, Quinn S, Nicolosi V, Kelly JM, Blau WJ, Coleman JN. Spontaneous debundling of single-walled carbon nanotubes in DNA-based dispersions. *J. Phys. Chem. C.* 2007;111:66–74.
38. Ishibashi A, Yamaguchi Y, Murakami H, Nakashima N. Layer-by-layer assembly of RNA/single-walled carbon nanotube nanocomposites. *Chem. Phys. Lett.* 2006;419:574–577.
39. Zhao XC, Johnson JK. Simulation of adsorption of DNA on carbon nanotubes. *J. Am. Chem. Soc.* 2007;129:10438–10445.
40. Li JL, Gershow M, Stein D, Brandin E, Golovchenko JA. DNA molecules and configurations in a solid-state nanopore microscope. *Nat. Mater.* 2003;2:611–615.
41. Zimmerli U, Koumoutsakos P. Simulations of electrophoretic RNA transport through transmembrane carbon nanotubes. *Biophys. J.* 2008;94:2546–2557.
42. Enyashin AN, Gemming S, Seifert G. DNA-wrapped carbon nanotubes. *Nanotechnology.* 2007;18:245702.

43. Fantini C, Jorio A, Santos AP, Peressinotto VST, Pimenta MA. Characterization of DNA-wrapped carbon nanotubes by resonance Raman and optical absorption spectroscopies. *Chem. Phys. Lett.* 2007;439:138–142.
44. Preuss M, Schmidt WG, Bechstedt F. Coulombic amino group-metal bonding: adsorption of adenine on Cu(110). *Phys. Rev. Lett.* 2005;94:236102.
45. Ebbesen TW. *Carbon Nanotubes: Preparation and Properties*. CRC Press, Boca Raton, FL, 1997.
46. Tersoff J, Hamann DR. Theory of the scanning tunneling microscope. *Phys. Rev. B.* 1985;31:805–813.
47. Hughes ME, Brandin E, Golovchenko JA. Optical absorption of DNA–carbon nanotube structures. *Nano Lett.* 2007;7:1191–1194.
48. Meng S, Wang WL, Maragakis P, Kaxiras E. Determination of DNA-base orientation on carbon nanotubes through directional optical absorbance. *Nano Lett.* 2007;7:2312–2316.
49. Murakami Y, Einarsson E, Edamura T, Maruyama S. Polarization dependence of the optical absorption of single-walled carbon nanotubes. *Phys. Rev. Lett.* 2005;94:087402.
50. Rajendra J, Rodger A. The binding of single-stranded DNA and PNA to single-walled carbon nanotubes probed by flow linear dichroism. *Chem. Eur. J.* 2005;11:4841–4847.
51. Daniel S, Rao TP, Rao KS, et al. A review of DNA functionalized/grafted carbon nanotubes and their characterization. *Sens. Actuators B.* 2007;122:672–682.
52. Chu S. Laser manipulation of atoms and particles. *Science.* 1991;253:861–866.
53. Smith SB, Finzi L, Bustamante C. Direct mechanical measurements of the elasticity of single dna-molecules by using magnetic beads. *Science.* 1992;258:1122–1126.
54. Kong J, LeRoy BJ, Lemay SG, Dekker C. Integration of a gate electrode into carbon nanotube devices for scanning tunneling microscopy. *Appl. Phys. Lett.* 2005;86:112106.
55. Rummel RM, Ziegler C. Room temperature adsorption of aniline (C₆H₅NH₂) on Si(100) (2 × 1) observed with scanning tunneling microscopy. *Surf. Sci.* 1998;418:303–313.
56. Rumelhart DE, Hinton GE, Williams RJ. Learning representations by back-propagating errors. *Nature.* 1986;323:533–536.